

# Effect of mean stress on high-cycle fatigue strength of IN 713LC superalloy

L. Kunz<sup>1\*</sup>, P. Lukáš<sup>1</sup>, R. Mintách<sup>2</sup>, K. Hrbáček<sup>3</sup>

<sup>1</sup>*Institute of Physics of Materials, ASCR, Žitkova 22, 616 62 Brno, Czech Republic*

<sup>2</sup>*Institute of Materials Science and Engineering, Faculty of Mechanical Engineering, Brno University of Technology, Technická 2896/2, 616 69 Brno, Czech Republic*

<sup>3</sup>*První Brněnská strojírna Velká Bíteš, a.s., Vlkovská 279, 595 12 Velká Bíteš, Czech Republic*

Received 27 June 2006, received in revised form 22 August 2006, accepted 24 August 2006

## Abstract

Fatigue strength of Ni base superalloy IN 713LC was experimentally determined at 800 °C in air using load controlled cycling with tensile mean stress. The constant fatigue life diagram has been constructed with particular attention to the influence of small stress amplitudes at high mean stresses. The mechanism of Stage I initiation of fatigue cracks, the role of casting defects and cavities and their effect on the fatigue strength have been discussed.

**Key words:** IN 713LC, high-cycle fatigue, constant fatigue life diagram, fatigue crack initiation

## 1. Introduction

Several schemes have been proposed for the safe design against fatigue at the presence of a mean stress. Gerber, Goodman, Haigh or Soderberg diagrams have been used in engineering practice since the beginning of the last century, e.g. [1–3]. These diagrams represent constant fatigue life charts for a combination of stresses (stress amplitude,  $\sigma_a$  and mean stress,  $\sigma_{\text{mean}}$ ) in such a way that the regions where fatigue failure will not occur, or will take place at a defined number of cycles, are demarcated. The constant fatigue life diagrams express the general observation that the fatigue lifetime at a given stress amplitude decreases with increasing tensile mean stress. Because the empirical determination of constant fatigue life diagrams is time consuming and expensive due to considerable experimental effort, it is not surprising that the data for many engineering alloys are not available either at all or not in sufficient extent. This holds also for Ni base superalloys at high temperatures. Moreover, the published constant lifetime curves are in general shown as lines, without experimental points (e.g. [3]); the scatter of relevant experimental data remains hidden.

Superalloys are employed in engineering practice for components mechanically loaded at high temperatures. A turbine wheel of a gas engine is an example of a component loaded with high tensile mean stress and superimposed cycling at high temperature. The tensile stress component is a result of centrifugal forces and bending moments from the streaming gas and the cycling comes from the inevitable vibrations. That is why the high-cycle fatigue resistance was the original fatigue property studied and developed for engineering use. Later on the research attention has been focused on the low-cycle fatigue and combination of low-cycle fatigue with creep (e.g. [4]) because significant loadings appear during start-up and shutdown of engines. The high-cycle fatigue data are less common than the low-cycle results [5].

Nickel base cast superalloy IN 713 and its variant IN 713LC are alloys employed in the aircraft gas turbine market. In spite of the application of IN 713 since the mid-1950s, leading European industrial companies are still interested in the more reliable characterization of the high temperature high-cycle fatigue properties. Because the casting defects substantially reduce the fatigue strength, “defect free” components are required in engineering practice. In reality it means

\*Corresponding author: tel.: 00420 549 246 327; fax: 00420 541 218 657; e-mail address: kunz@ipm.cz

that the defect size is not allowed to exceed a critical size given by the resolution limit of defectoscopic methods, which is usually some tenths of a millimetre. On the other hand, the large scatter of experimental high cycle S-N data indicates that the effect of defects remains even in the nominally “defect free” alloy. Inherence of imperfections is an inevitable problem not only of conventionally cast superalloys, but shrinkage porosity and individual pores can be found in Ni base single crystals cast into temperature gradient as well.

Crystallographic crack initiation with extraordinary long Stage I and crystallographic crack propagation are common features of all Ni base superalloys at room and at high temperatures. Extensive Stage I cracking has been reported many times both for the cast polycrystalline alloys and for single crystals [6]. Crystallographic facets have been often observed on fatigue fracture surfaces. River lines, fracture steps and equiaxed dimples are typical morphological features. Casting defects are frequently situated at the crack initiation site [7–9]. The crystallographic fracture surface is typical for low fatigue crack propagation rate (usually below  $10^{-5}$  mm/cycle), see e.g. [10]. Details of the fracture mode depend on the stress ratio of minimum to maximum stress in a loading cycle [11]. Ni base superalloys are face-centered cubic alloys and thus the deformation takes place on  $\{111\}$  planes. The facets are often called cleavage facets and they follow the  $\{111\}$  planes. The cracking due to the heterogeneous planar slip on the  $\{111\}$  planes in  $\langle 110 \rangle$  directions is general and was observed not only under symmetrical fatigue loading but e.g. also on notched single crystals subjected to far-field compression [12]. The remarkable scatter of S-N data of cast superalloys seems to be related not only to the existence of defects, but also with the extraordinary long Stage I crystallographic crack initiation.

The aim of this work was to determine the lifetime diagram of a conventionally cast IN 713LC at 800°C. Special attention was paid to the influence of small high-cycle vibrations on the lifetime. Fractographic observation has been accomplished with the view to shed light on the influence of defects and crystallographic Stage I crack initiation on the fatigue strength.

## 2. Material and experiments

Polycrystalline superalloy IN 713LC was cast by the company PBS Velká Bíteš, a. s. The semiproducts for specimen preparation were conventionally cast rods of 20 mm in diameter and of 100 mm in length. Cylindrical button-end specimens of 5 mm in diameter and with 35 mm long gauge length were machined from the rods. The final operation was a fine grinding.

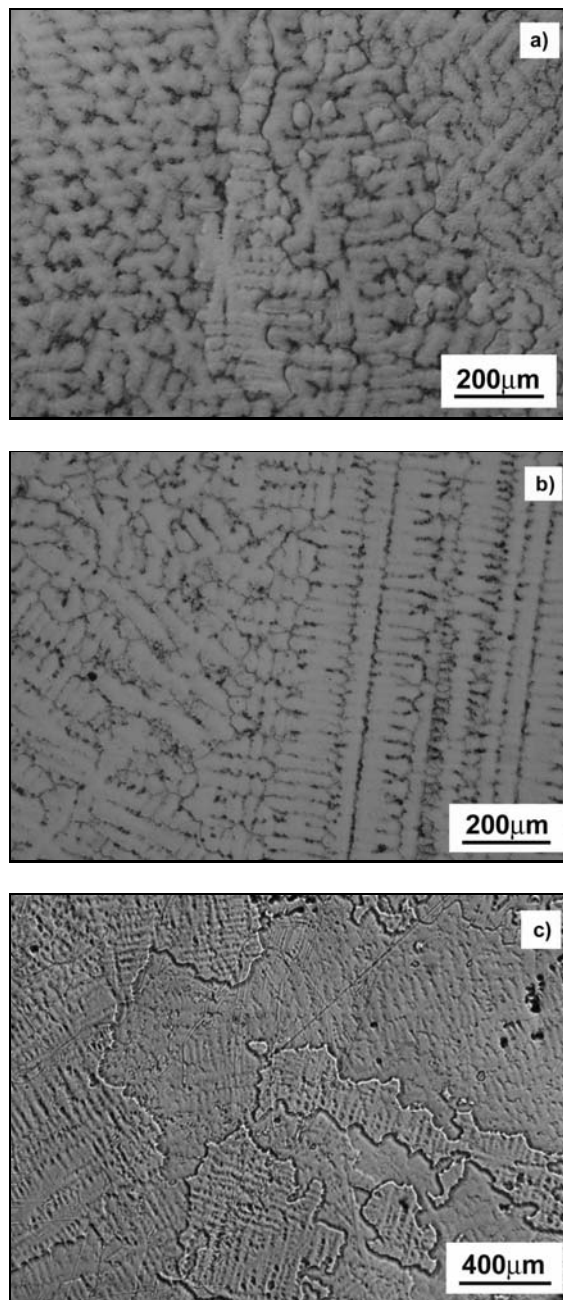


Fig. 1. Microstructure of IN 713LC, light microscopy. a) Long dendrites in axial section, b) dendrites in transversal section, c) grain morphology in transversal section.

The cast microstructure is dendritic in nature, Fig. 1. Dendrites with long primary arms can be observed in the axial section of rods, Fig. 1a. The structure in the transversal section can be seen in Fig. 1b. Figure 1c shows that the grain size in the transversal section of the cast rod is of the order of millimetres. The microstructure as revealed by scanning electron microscopy on the etched surfaces is shown in Fig. 2. Dendritic regions with regular  $\gamma/\gamma'$  microstructure, interdendritic areas with small cavities, voids, casting

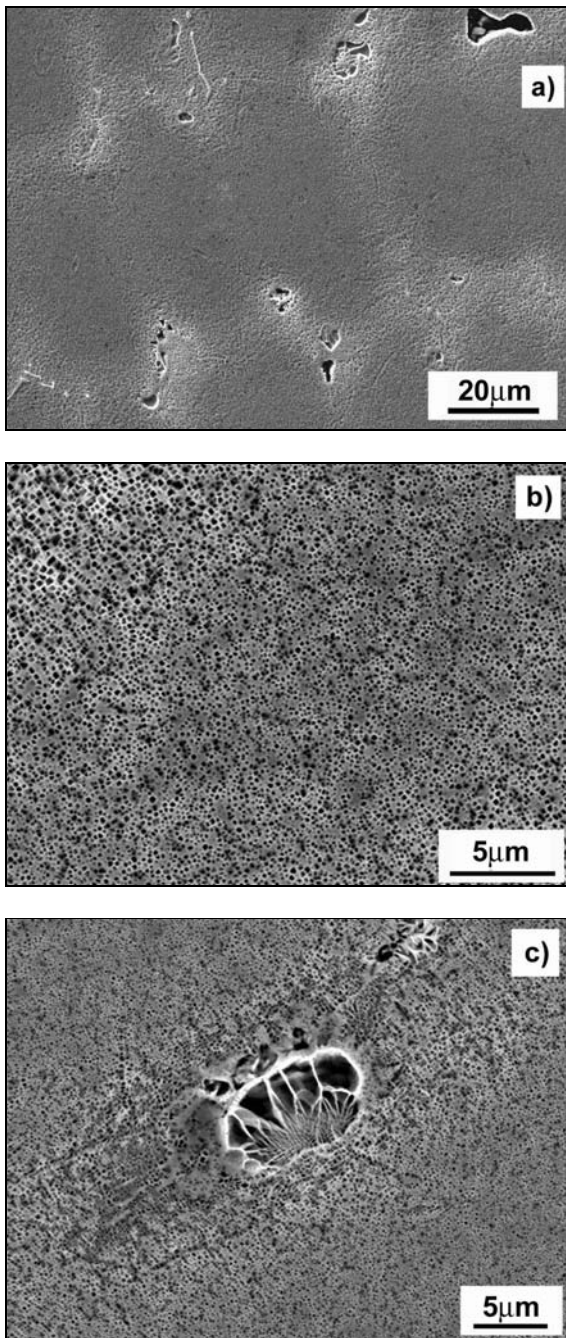


Fig. 2. Microstructure of IN 713LC, scanning electron microscopy. a) Dendritic and interdendritic regions, b) fine regular  $\gamma/\gamma'$  microstructure in a dendritic region, c) colony of irregular  $\gamma'$  particles embedded in the fine  $\gamma/\gamma'$  microstructure.

defects, carbides and colonies of large and irregular  $\gamma'$  particles can be seen in Fig. 2a. The dendritic regions are characteristic with very fine regular  $\gamma/\gamma'$  microstructure, Fig. 2b. An example of a colony of irregular  $\gamma'$  particles embedded in the fine  $\gamma/\gamma'$  microstructure is shown in Fig. 2c.

High temperature fatigue tests at 800°C were con-

ducted at controlled load in a 100 kN resonant fatigue testing machine. The controlled load parameters were the load amplitude and the mean load. The frequency of sine-wave loading was  $105 \pm 3$  Hz. The start-up procedure of a fatigue test consisted of heating-up the specimen in a high temperature furnace. The mean load during the heating was held equal to zero. After two hours the mean load was applied and then the resonant cycling was switched on. The start-up of the resonant cycling was characterized by a loading ramp of a length of about 500 cycles. The temperature gradient on the specimen gauge length was smaller than  $3^\circ\text{C}/\text{cm}$  and the temperature maximum was in the central part of the gauge length. The long-term temperature stability was within  $\pm 1^\circ\text{C}$ . Fatigue tests were conducted in laboratory air.

Fracture surfaces and microstructure were observed by means of JEOL JSM 6460 scanning electron microscope.

### 3. Results

The S-N fatigue data in the high-cycle fatigue region for load symmetrical cycling can be seen in Fig. 3. The fatigue test results can be expressed by two lines, one of which is a horizontal line characterizing the fatigue limit  $\sigma_c = 160$  MPa. The line is based on three run-out specimens at the number of cycles exceeding  $10^7$ . The second line in semilogarithmic co-ordinates is the best fit of experimental points corresponding to the broken specimens:

$$\sigma_a = 716N_f^{0.091}, \quad (1)$$

where stress amplitude,  $\sigma_a$ , is in MPa and  $N_f$  is the number of cycles to fracture. The coefficient of determination  $R$  of the best fit is 0.73. The number of

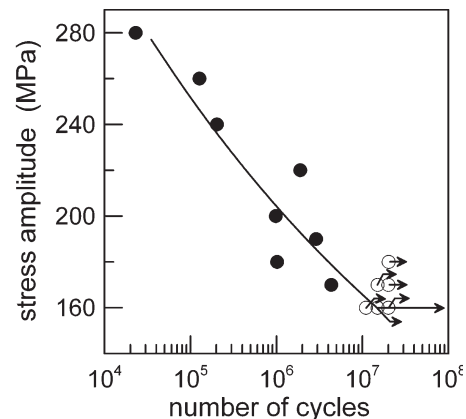


Fig. 3. S-N curve for symmetrical loading.

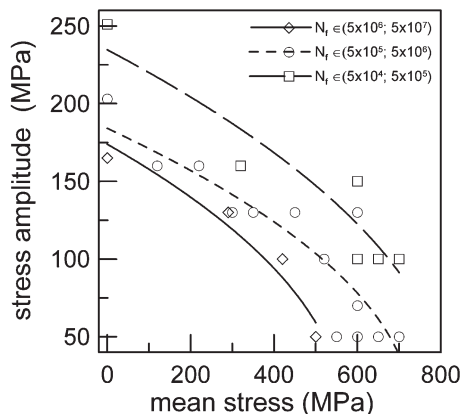


Fig. 4. Constant fatigue life diagram.

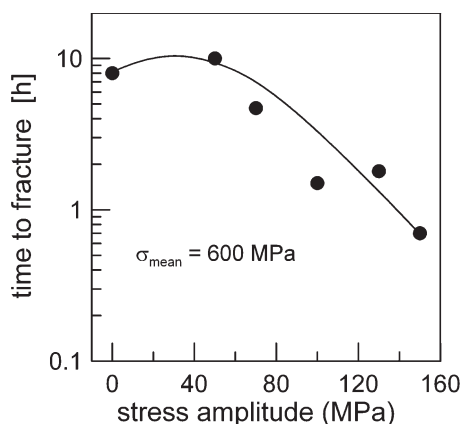


Fig. 5. Dependence of time to fracture on the stress amplitude for cyclic loading with the mean stress of 600 MPa.

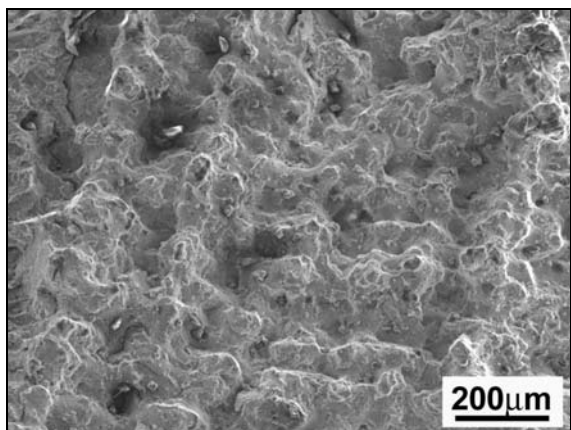


Fig. 6. Fracture surface of a specimen ruptured at the stress of 600 MPa.

cycles to fracture exhibits a considerable scatter. For example, at the stress amplitude of 180 MPa two specimens were tested. One of them failed after  $10^6$  cycles, while the second one endured  $2 \times 10^7$  cycles without failure.

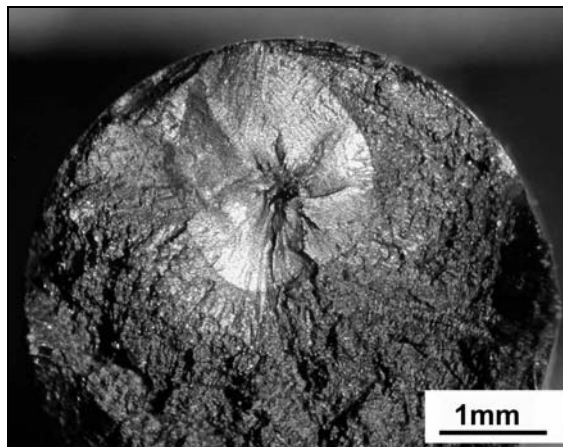


Fig. 7. Initiation of a fatigue crack on a large internal casting defect followed by transcrystalline crack propagation. Mean stress 350 MPa, stress amplitude 130 MPa.

Experimentally determined constant fatigue life diagram is shown in Fig. 4. The points for the symmetrical cycling were calculated according to the Eq. (1). Other experimental points represent particular measurements for given combination of stress amplitude and the mean stress. Distinct points distinguish the fatigue life in such a way that intervals from  $5 \times 10^4$  to  $5 \times 10^5$ ,  $5 \times 10^5$  to  $5 \times 10^6$  and  $5 \times 10^6$  to  $5 \times 10^7$  cycles to fracture can be taken from the diagram. The experimental points exhibit a scatter, which is inherent to the cast alloys. Nevertheless, the experimental data enable to construct lines denoting the reasonable estimates for fatigue lives of  $10^5$ ,  $10^6$  and  $10^7$  cycles. The lines in Fig. 4 correspond to the Gerber parabola fitted to the experimental points; the corresponding coefficients of determination are 0.97 for the curve characterizing the life  $10^7$  cycles, 0.80 for  $10^6$  and 0.87 for  $10^5$  cycles.

Figure 5 shows the influence of the stress amplitude on the fatigue life for the constant mean stress in terms of the time to fracture. Cycling with the stress amplitude of 50 MPa superimposed on the mean stress of 600 MPa results in fracture after 10 h (which corresponds to the number of cycles  $3.7 \times 10^6$ ), whereas the loading with zero stress amplitude, i.e. pure creep loading, results in shorter lifetime of about 8 h. For the stress amplitudes exceeding 50 MPa, however, it can be seen that the trend is reversed and a decrease of time to fracture with increasing  $\sigma_a$  is obvious.

Fractographic observation provides the following picture. The typical fracture surface corresponding to the creep loading is of a ductile type. Fracture surface morphology reflects often dendritic structure. An example of such a region is shown in Fig. 6. Fracture surfaces corresponding to the maximum on the  $t_f$  vs.  $\sigma_a$  diagram or to the decreasing part of the diagram exhibit three distinct types of fracture. The first type

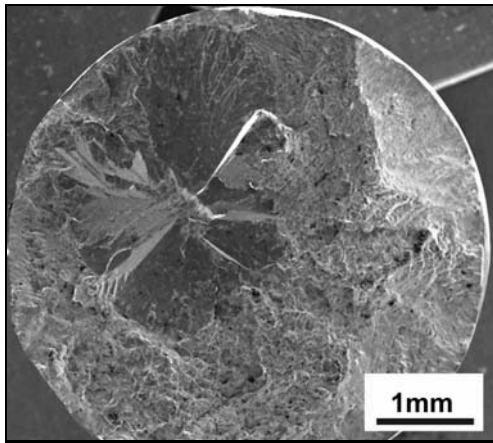


Fig. 8. Crystallographic facets adjacent to the casting defect.

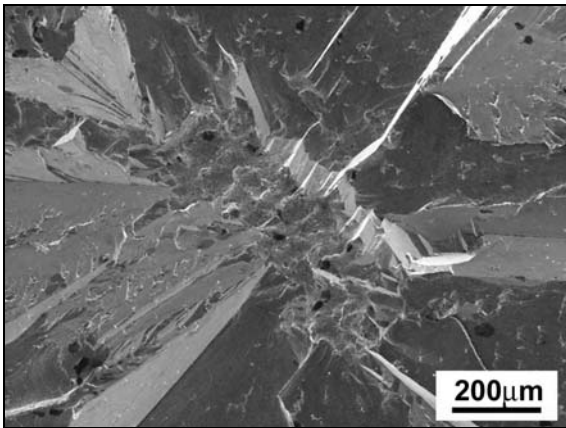


Fig. 9. Crystallographic facets starting from the casting defect. Detail from Fig. 8.

can be seen in Fig. 7. The fatigue crack started from a relatively large internal casting defect. Its dimension of some tenths of millimetre is just on the resolution limit of conventional defectoscopy. The fatigue crack propagated from the defect in a plane macroscopically perpendicular to the maximum stress. A clear “fish eye” can be seen. The fatigue crack propagation was transcrystalline. The crack surface appearance under small magnification changed suddenly when the crack reached the surface and the laboratory atmosphere interfered with the freshly created fatigue fracture surface. The second type of crack initiation is shown in Fig. 8. Crystallographic facets of mirror appearance adjacent to the casting defect can be seen. They are mutually inclined at high angles and at low magnification they have high reflectivity. At higher magnification they are shown in Fig. 9. Crystallographic facets pass to the noncrystallographic fracture surface in longer distance from the central casting defect; this

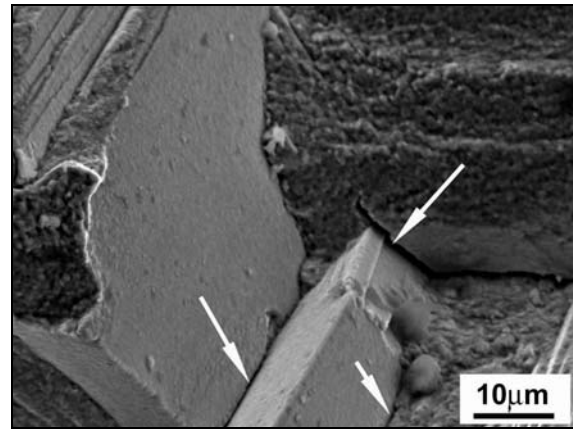


Fig. 10. Transition from crystallographic to noncrystallographic fracture. Arrows indicate decohesion.

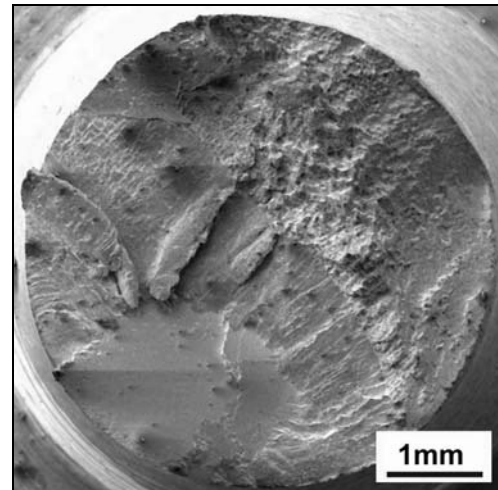


Fig. 11. Crystallographic facet starting from the specimen surface and transition to the noncrystallographic fatigue crack propagation. Mean stress 0 MPa, stress amplitude 170 MPa.

distance is of about 1 mm in Fig. 8. An example of the transition from crystallographic to noncrystallographic fracture is shown in Fig. 10. Crystallographic fracture planes are flat and do not exhibit any apparent morphological details related to the material microstructure. A decohesion between facets, marked by arrows, can be very often observed. The spacing between facets makes some microns. The upper arrow in Fig. 10 denotes a short, evidently noncrystallographic crack, which accommodates the decohesion between the facets marked by the bottom arrows. The noncrystallographic fracture surface (at the top right) is rough when compared to the facet surface and is covered by small bulges. Their dimension corresponds roughly to the characteristic dimension of  $\gamma/\gamma'$  microstructure in dendritic areas. The third type of crack

initiation observed differs by the absence of an apparent defect. Crystallographic facets in this case do not exhibit any relation to the structure imperfections and often start from the specimen surface. Later on they pass to the noncrystallographic fracture surface as in the preceding case. An example is shown in Fig. 11.

#### 4. Discussion

Considerable scatter of fatigue life is inherent to the conventionally cast IN 713LC superalloy. Nevertheless, for a material, which does not contain defects exceeding the resolution limit of conventional defectoscopic methods, plausible constant fatigue life diagram can be experimentally determined. For high mean stresses and superimposed small stress amplitudes of frequency of 105 Hz an increase of lifetime was observed. The dependence of  $t_f$  on  $\sigma_a$  is non-monotonous. This observation corresponds to the old experimental results showing a “nose” on  $\sigma_a$ - $\sigma_{mean}$  constant fatigue lifetime diagrams of heat resistant alloys in the high mean stress region [13, 14]. Because an increase of relative time to fracture due to the influence of small stress amplitudes was reported also for smooth and notched CMSX-4 and CM186LC single crystals [9, 15], this seems to be a common feature of the high temperature high-frequency loading of Ni-base superalloys.

The initiation mechanism of fatigue cracks in IN 713LC can be of three different types. Cracks may start on casting defects either at the surface or in the interior of a cast component and propagate right from the beginning in a noncrystallographic manner by Stage II mode in a plane nearly perpendicular to the principal stress. This type of crack propagation was observed in the case of presence of large casting defects or shrinkage porosities, having usually dimensions above the resolution limit of defectoscopic methods. No distinct features were observed on the Stage II fracture surface. Indeed, the fatigue strength depends on the defect size, which is further reflected by the scatter of S-N data.

Basically, the most important crack initiation mechanism is the Stage I cracking. This type of initiation is often in an apparent relation to the casting pores or smaller defects, which are below the resolution limit of conventional defectoscopic methods. This has been reported e.g. in [7] and corresponds to our fractographic observation on IN 713LC, Fig. 8. On the other hand, in many cases no apparent interaction between the crystallographic facet and pores can be detected. An example is shown in Fig. 12. Flat crystallographic facet intersects the shrinkage porosity without any sign of the development of a plastic deformed zone. Particularly the small pores (marked by A and B) obviously cut by the crystallographic plane

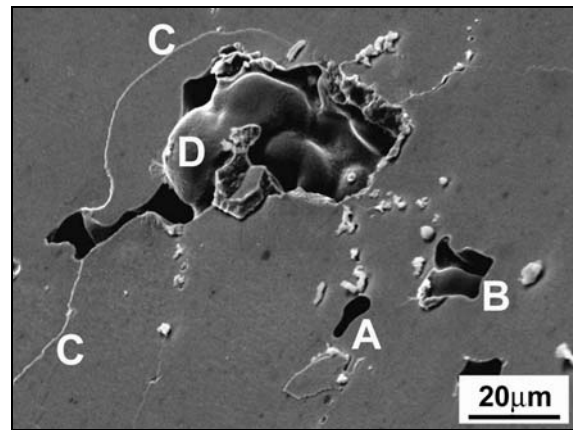


Fig. 12. Crystallographic facet. A, B – small casting pores, C – steps on the facet, D – shrinkage surface rising above the plain of facet.

without any apparent strain concentration support the idea of decohesion along this plane. Simultaneously, no evidence of rubbing can be seen in Fig. 12. Sharp, not damaged steps are visible at the fracture surface (marked C) as well as parts of shrinkage surface rising clearly above the plain of decohesion (marked by D).

Slip-band decohesion model has been proposed for the explanation of the crystallographic crack growth by Duquette et al. [7] more than three decades ago. The Stage I fatigue cracking is based on the weakening of slip planes coplanar with the crack tip, and subsequent failure proceeds by a combination of local normal and shear stress. The crack propagates along the  $\{111\}$  plane. Obrtlík et al. [16] and recently Petreñec et al. [17] studied the localization of the cyclic plastic deformation in IN 713LC in a broad temperature interval. They observed highly inhomogeneous dislocation arrangement and development of dislocation-rich slabs in the form of thin bands and ladder-like bands parallel to the  $\{111\}$  planes passing through the  $\gamma$  matrix and  $\gamma'$  precipitates. Formation of persistent slip bands running through the  $\gamma$  matrix and  $\gamma'$  precipitates both in dendritic and eutectic regions were observed in single crystals of CMSX-4 and CM 186LC at 850 °C fatigued at high tensile mean stress [8]. Persistent slip bands lying along the traces of the  $\{111\}$  crystallographic planes producing a “zig-zag” path, which may be the nucleus of a fatigue crack, were documented in [18].

The experimentally observed large scatter of S-N data can be rationalized in the following way. The crack initiation Stage I in many engineering alloys terminates usually after some microns of propagation along the slip plane inclined approximately 45° to the direction of the applied stress. Then follows the transition to the Stage II propagation perpendicular to the principle stress. In cast Ni base superalloys typically occurs heterogeneous cyclic slip activity on

the {111} planes. The dimension of active planes is of the order of millimetres. Persistent slip bands represent weakened planes, which are suitable for decohesion. The decohesion due to cycling results in a formation of internal cracks which may substantially differ by size. The dimension, orientation and the spacing between the crystallographic facets (see Fig. 10) are dependent on the microstructure and on the intensity of the slip activity in the neighbouring persistent slip bands. That is why the fatigue lifetime of particular specimens can vary substantially. The slip activity on suitably oriented {111} planes may be supported by larger casting inhomogeneities due to their stress concentration effect. On the other hand, the persistent slip band being once active, can intersect smaller casting pores without any signs of additional plasticity and the decohesion takes place in a manner shown in Fig. 12. From this point of view the most decisive for the crack initiation seems to be the slip activity in persistent slip bands and their “length”; small casting defects, usually below the resolution limit of the defectoscopic methods seem to be irrelevant to the fatigue crack initiation.

## 5. Conclusions

The constant fatigue life diagram of IN713 LC has been experimentally determined for temperature of 800°C and loading in laboratory air.

Small cyclic component of 105 Hz frequency superimposed on the mean stress is safe and does not reduce the lifetime. The time to fracture even increases with increasing stress amplitude. The reverse of this trend is determined by the change of damage mode from ductile to fatigue that occurs with increasing HCF amplitudes.

High scatter of S-N data and experimental points of constant lifetime diagram were explained by the presence of casting defects and long Stage I fatigue crack initiation. The fractographic observation supports the slip band decohesion model of crack initiation and the decisive role of persistent slip bands in fatigue crack nucleation.

## Acknowledgements

This work was financially supported by the Grant agency of the Czech Republic under the contract 106/05/2112. This support is gratefully acknowledged.

## References

- [1] HEYWOOD, R. B.: *Designing Against Fatigue*. London, Chapman and Hall 1962.
- [2] SURESH, S.: *Fatigue of Materials*. Cambridge, Cambridge University Press 1998.
- [3] BUCH, A.: *Fatigue Data Handbook*. Zürich, Trans Tech Publications Ltd. 2000.
- [4] ZRNÍK, J.—SEMEŇÁK, J.—HORŇÁK, P.—VRCHOVINSKÝ, V.: *Kovove Mater.*, 43, 2005, p. 93.
- [5] DONACHIE, M. J.—DONACHIE, S. J.: *Superalloys. A Technical Guide*. 2<sup>nd</sup> Edition. Materials Park OH, ASM Int. 2002, p. 255.
- [6] ANTOLOVICH, B. F.: In: *ASM Handbook Fatigue and Fracture*. Vol. 19. Materials Park OH, ASM Int. 1996, p. 854.
- [7] DUQUETTE, D. J.—GELL, M.—PITEO, J. W.: *Met. Trans.*, 1, 1970, p. 3107.
- [8] MacLACHLAN, D. W.—KNOWLES, D. M.: *Fat. Fract. Engng. Mater. Struct.*, 24, 2001, p. 425.
- [9] LUKÁŠ, P.—KUNZ, L.—SVOBODA, M.: *Int. J. of Fatigue*, 27, 2005, p. 1535.
- [10] YU, W.—YUAN, J.—WANG, Z.: *Fat. Fract. Engng. Mater. Struct.*, 9, 1987, p. 425.
- [11] MERCER, C.—SOBOYEJO, A. B. O.—SOBOYEJO, W. O.: *Acta Mater.*, 47, 1999, p. 2727.
- [12] ASWATH, P. B.: *Met. and Mat. Transactions A*, 25A, 1994, p. 287.
- [13] VITOVEC, F. H.: *Dynamic Creep*. Proc. Amer. Soc. Test. Mat., 57, 1957, p. 977.
- [14] FORREST, P. G.: *Fatigue of Metals*. Oxford, Pergamon Press 1962.
- [15] LUKÁŠ, P.—KUNZ, L.—SVOBODA, M.: *Zeitschrift für Metallkunde*, 93, 2002, p. 661.
- [16] OBRTLÍK, K.—MAN, J.—PETRENEC, M.—POLÁK, J.: In: *Fatigue 2002*. Vol. 2/5. Proc. of the 8<sup>th</sup> Int. Fatigue Congress. Ed.: Blom, A. F. Stockholm, Emas Publishing 2002, p. 963.
- [17] PETRENEC, M.—OBRTLÍK, K.—POLÁK, J.: *Mat. Sci. Eng. A*, 400–401, 2005, p. 485.
- [18] LUKÁŠ, P.—KUNZ, L.—SVOBODA, M.: *Mater. Sci. Eng. A*, 387–389, 2004, p. 505.